

Vortex Emission Accompanies the Advection of Optical Localized Structures

F. Haudin,¹ R. G. Rojas,² U. Bortolozzo,¹ M. G. Clerc,³ and S. Residori¹

¹*INLN, Université de Nice-Sophia Antipolis, CNRS, 1361 route des Lucioles 06560 Valbonne, France*

²*Instituto de Física, Pontificia Universidad Católica de Valparaíso, Casilla 4059, Valparaíso, Chile*

³*Departamento de Física, FCFM, Universidad de Chile, Casilla 487-3, Santiago Chile*

(Received 8 October 2010; revised manuscript received 29 December 2010; published 10 February 2011)

We show that the advection of optical localized structures is accompanied by the emission of vortices, with phase singularities appearing in the wake of the drifting structure. Localized structures are obtained in a light-valve experiment and made to drift by a mirror tilt in the feedback loop. Pairs of oppositely charged vortices are detected for small drifts, whereas for large drifts a vortex array develops. Observations are supported by numerical simulations and linear stability analysis of the system equations and are expected to be generic for a large class of translated optical patterns.

DOI: [10.1103/PhysRevLett.106.063901](https://doi.org/10.1103/PhysRevLett.106.063901)

PACS numbers: 42.65.-k, 05.45.-a, 45.70.Qj

In hydrodynamics, fluid particles or scalar passive quantities can be advected by a flow in a given direction. A classical example of the advection phenomenon and resulting instabilities is that of Bénard–von Kármán street, where a viscous fluid flowing past an obstacle organizes in two rows of eddies on either side of its wake, with the vortices on one side rotating in one sense and those on the other side rotating oppositely [1]. Such behavior is driven by the Reynolds number, a dimensionless parameter that includes the advection velocity, characteristic length of the obstacle and fluid viscosity. In non dissipative systems, like superfluids and Bose-Einstein condensates, vortex shedding from a moving obstacle has been evidenced by numerical simulations of the nonlinear Schrödinger equation [2,3], showing several analogies with vortex streets in Newtonian fluids [4].

The formation of vortex-antivortex pairs, or topological defects, also accompanies phase transitions that are associated with symmetry breaking [5], such as, for example, in magnets, superfluids [6], plasma jets [7]. In optics, vortices have been introduced on symmetry grounds as the topological defects arising above the laser transition [8]. In this context, they have been identified as the singular points where the field amplitude is zero, while the circulation of the phase gradient on any loop which encloses the vortex core is equal to $\pm 2\pi$, with the total vorticity a conserved quantity. Optical vortices, therefore, appear and disappear in pairs of opposite charge. They are also known as screw dislocations or phase singularities, because the phase is twisted around the axis of light propagation, with the topological charge corresponding to the number of twists that the light makes in one wavelength [9]. In nonlinear optics, vortex-antivortex pairs have been reported for photorefractive cavities [10–12] and Kerr media [13]. By introducing a mirror tilt in a photorefractive cavity, a wake of alternating vortices has been observed in the transverse field [14], showing analogies with fluid behaviors. Indeed, nonlinear light often behaves as a “photon

fluid” and several analogies with hydrodynamics exist, including, for instance, shock waves [15], wave turbulence [16] and rogue waves [17,18]. In this framework, optical localized structures are intriguing objects, having both wave properties, described by the amplitude of the electric field, and a particlelike nature, permitting to switch them on or off as elementary pixels [19]. Optical vortices have been observed in triangularly shaped localized structures [20], where the breaking of the circular symmetry was shown to cause the appearance of several pairs of oppositely charged phase singularities [21].

In this Letter, we show that, in the presence of a translational effect that makes them to drift, optical localized structures are advected as particlelike objects and, while they are advected, the $O(2)$ rotational symmetry is broken leading to a distortion of their initially round profile and to the emission of vortices by pairs of oppositely charged phase singularities in their wake. We obtain localized structures in the liquid crystal light-valve (LCLV) experiment [22] and make them to drift by introducing a mirror tilt in the optical feedback loop. Phase singularities are detected by an interferometric system allowing their visualization as dislocations in a fringe pattern. Qualitative analogies are drawn with vortex street in viscous fluids, while the dual nature of optical localized structures brings us to emphasize the role of symmetry breaking as a cause of the vortex appearance. For large translations, we show that structures form a chain and develop a regularly spaced vortex array. Observations are confirmed by numerical simulations and qualitatively accounted for by linear stability analysis of the full model for the LCLV with translated optical feedback.

Previous studies of translational effects in the LCLV experiment have evidenced secondary instabilities of patterns [23,24] such as transitions from hexagons to stripes, squares to zigzag [25]. More recently, it has been shown that drifting localized structures can be guided by using a spatial light modulator [26]. However, the drift-induced

asymmetrical deformation of localized structures and the associated emission of vortices have never been reported or predicted before. When a translational effect is introduced in the experiment by tilting the mirror at the entrance of the feedback loop (see Fig. 1), localized structures start to drift along the direction of the mirror displacement. The motion of a single localized structure is shown in Fig. 1(a), where successive experimental snapshots with interference fringe patterns are displayed with a time separation of 1.07 s. Here, the drifting direction x is marked by an arrow. After the initial transient acceleration induced by the mirror tilt, the localized structure acquires a constant velocity, as indicated by the dotted line. During the first stages of the advection, the structure loses its round shape and undergoes an asymmetrical deformation developing a large tail in its wake. The fourth panel of Fig. 1(a) shows a profile of an advected structure without fringes. The symmetry breaking is accompanied by the emission of pairs of optical vortices, appearing as dislocations in the interference pattern.

To visualize phase singularities the setup is modified in such a way to include a Mach-Zehnder type interferometer, as shown in Fig. 1(b). At this purpose a reference beam is extracted by the cube splitter PC and sent through mirrors m to interfere with a small portion of the feedback beam. The resulting interference pattern is sent to a CCD camera, where fringes are recorded and phase singularities detected as dislocations. In order to maximize the fringe contrast, the relative intensity and polarization of the reference and signal beam are adjusted by a neutral density filter and a half-wave plate, respectively. The LCLV is made of a thin

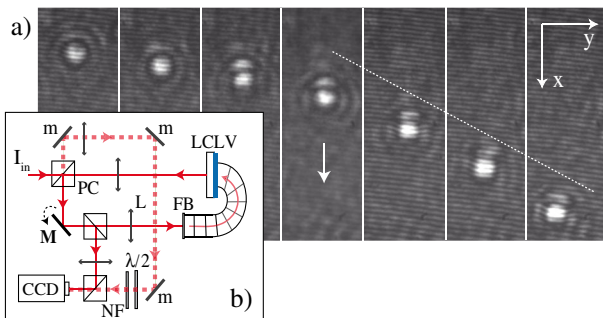


FIG. 1 (color online). (a) Successive experimental snapshots (time separation 1.07 s) of an optical localized structure drifting along the x direction; the advection occurs after tilting the mirror M at the entrance of the feedback loop; the first three snapshots realize the process of symmetry breaking whereas the last four account for the propagative phenomenon; the dotted line is the velocity acquired after the initial acceleration; (b) experimental setup: FB optical fiber bundle, L lenses, PC polarizing cube splitter; the other cubes deflect part of the beam to the CCD camera for detection; a reference beam (dashed line) is used to realize a Mach-Zehnder interferometer through mirrors m ; the half-wave plate, $\lambda/2$, and the neutral density filter, NF, adjust the polarization, respectively, the intensity of the reference beam.

nematic liquid crystal (LC) layer, 15 μm thickness, sandwiched between a glass plate and a photoconductive wall over which a dielectric mirror is deposited. The surfaces in contact with the LC are treated in such a way to induce a planar anchoring of the molecules (nematic director parallel to the confining walls). A voltage V_0 is applied across the cell, which is illuminated by an expanded He-Ne laser beam, $\lambda = 632.8$ nm, linearly polarized along the vertical direction. Once passed through the LC, the beam is reflected back by the dielectric mirror deposited on the rear side of the valve and sent in the feedback loop. An optical fiber bundle is used to close the loop and redirect the beam back to the photoconductive side of the LCLV. The nematic director is oriented at 45° and the polarizing cube splitter PC introduces polarization interference between the ordinary and extraordinary waves, a condition ensuring the bistability between differently orientated states of the LC [27].

A self-imaging configuration is realized by inserting two cofocal lenses, $f = 25$ cm focal length, in such a way that the rear and the front side of the LCLV are conjugate planes. If the fiber bundle is displaced over a L distance from this self-imaging configuration, diffraction is introduced over L , thus selecting a transverse spatial scale $\sqrt{2\lambda L}$ that gives the size of localized structures. To optimize the vortices visualization, we have taken $L = -16$ cm, in order to have large localized structures (transverse diameter ≈ 450 μm), and the interferometer is adjusted to have about three to five fringes per structure. Figure 2(a) shows a zoom of the interference pattern around a moving structure. The snapshot is taken after a few seconds of the mirror tilt and the drift velocity can be roughly estimated as $v_d \approx 0.9$ mm/s. The fringe pattern is displayed with inverted intensity levels, over which are superimposed digitized fringe maxima. Oppositely charged phase singularities, marked by + and -, appear as pairs of dislocations in the wake of the moving structure. In Fig. 2(b) it is displayed a one-dimensional transverse profile of the drifting structure, from which the asymmetric deformation and tail development can be appreciated.

To confirm the observations we have performed numerical simulations of the full model for the LCLV

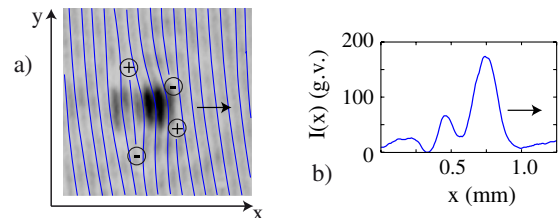


FIG. 2 (color online). (a) Experimental snapshot with inverted intensity levels and digitized fringe maxima showing a localized structure moving along the arrow direction; oppositely charged phase singularities, marked by + and -, appear as dislocations; (b) corresponding one-dimensional profile.

with translated feedback, which consists in two coupled equations, one for the average tilt angle θ of the LC [27]

$$\frac{2}{\pi}(\tau\partial_t\theta - l^2\nabla_{\perp}^2\theta + \theta) = 1 - \sqrt{\frac{V_{FT}}{\Gamma V_0 + \alpha I_w(x + \Delta x, y)}}, \quad (1)$$

with $\tau = 30$ ms and $l = 30$ μm the LC response time and, respectively, electrical coherence length, ∇_{\perp}^2 the transverse Laplacian, V_{FT} the Fredericksz transition voltage, Γ the transfer function of the equivalent electric circuit of the LCLV, V_0 the applied voltage, α a coefficient accounting for the response of the photoconductor and Δx the translation of the feedback beam, and one for the intensity I_w on the photoconductor

$$I_w(x) = \frac{I_{in}}{4} |e^{iL\nabla_{\perp}^2/2k}(e^{-i\varphi} - 1)|^2 \quad (2)$$

with $k = 2\pi/\lambda$ the optical wave number and $\varphi = \beta\cos^2\theta$ the phase shift acquired by the light when passing through the LC layer, $\beta = 4\pi\Delta n d/\lambda$, $\Delta n = 0.2$ the LC birefringence and d the thickness the LC layer. The electric field at the exit of the LC layer is $E_{in}(e^{-i\varphi} - 1)$, where E_{in} is the input field and $I_{in} = |E_{in}|^2$. Numerical integrations of Eqs. (1) and (2) are made by using a pseudo spectral method, for which the spatial derivatives and the diffraction operator are solved in Fourier space, while the temporal derivate is calculated with an adaptive Runge-Kutta algorithm. In the bistable regime a single localized structure is generated by applying a Gaussian pulse, then, a translation Δx of the intensity I_w is introduced.

Figure 3 shows a set of numerical results for $L = -16$ cm, $\alpha I_{in} = 1.2$, $V_0 = 12.9$ V, giving localized structures with a diameter of 450 μm . The range of Δx for which the advection regime exists is in between 30–250 μm . The intensity profiles show how the initially axisymmetric structure [$\Delta x = 0$, Fig. 3(a)] is deformed during the advection. For relatively small translations ($\Delta x = 126$ μm , Fig. 3(b)), the profile is slightly deformed, with wavelets visible behind the structure. For larger drifts [$\Delta x = 182$ μm , Fig. 3(c)], the deformation becomes more important, with the amplitude of the principal and secondary maxima increasing and a large wake developing behind the structure. At the left of the central panels are displayed linear intensity profiles along the drift direction. By numerically inspecting the electric field of the advected structures, phase singularities are detected as the intersections of the null lines of the real and imaginary parts, as displayed at the right of the central panels. While at rest the null lines of the electric field are circular and never cross each other, the deformation induced by the translation brings the lines to intersect at multiple points, where optical vortex are nucleated by pairs of opposite topological charge. In Fig. 4(a) the numerically calculated drift velocity v_d is plotted vs the drift Δx .

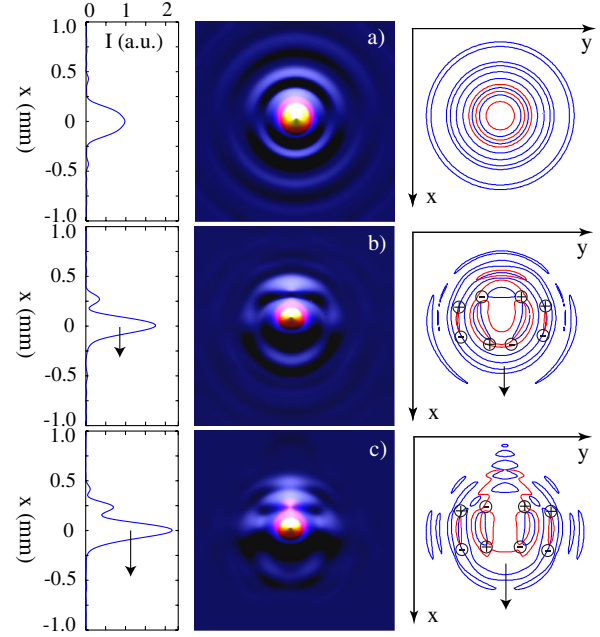


FIG. 3 (color online). Numerical intensity profiles of a drifting localized structure, (a) $\Delta x = 0$, (b) $\Delta x = 126$ μm , (c) $\Delta x = 182$ μm ; on the right, corresponding one-dimensional profiles along the advection direction x ; on the left, null lines of the electric field; dark (blue online), light (red online) lines corresponds to real, respectively, imaginary part of the field; phase singularities are nucleated at the intersections.

For further increase of the drift a change of the dynamical scenario is observed: while they are advected, localized structures form a chain and develop a spatial organization of regularly spaced vortices lining up in the direction of the drift. An experimental snapshot showing the chain and associated vortex array is displayed in Fig. 4(b). Figure 4(c) shows a numerical simulation for the same set of parameters as before and $\Delta x = 253$ μm . The null lines of the field, superimposed to the inverted intensity pattern, show a periodic array of intersections, at which

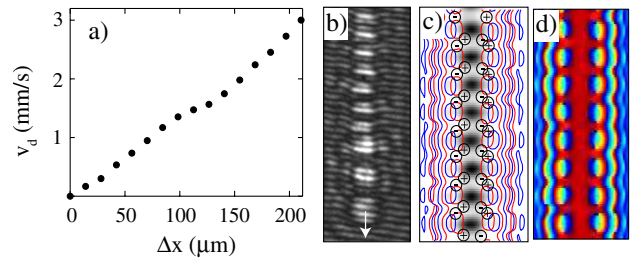


FIG. 4 (color online). (a) Numerically calculated advection velocity v_d vs the translation Δx ; $L = -16$ cm. (b)–(d) Chains of localized structure: (b) experimental interference pattern; (c) numerical intensity pattern for $\Delta x = 253$ μm with superimposed null lines of the electric field; dark (blue), light (red) lines corresponds to real, respectively, imaginary part of the field; (d) corresponding phase pattern, where dark (blue), light (red) intensity maps a phase change from $-\pi$ to π .

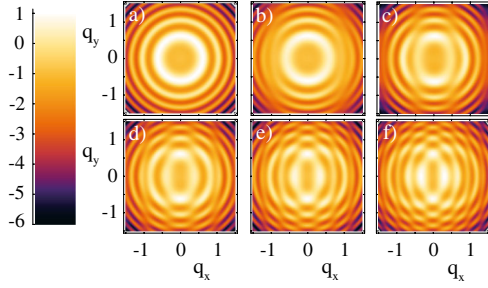


FIG. 5 (color online). Dispersion relation $\Re(\sigma)$ vs q_x, q_y for a Δx of (a) 0, (b) 50, (c) 100, (d) 150, (e) 200, (f) 250 μm .

phase singularities are nucleated by opposite pairs. The corresponding phase pattern is plotted in Fig. 4(d). The drift velocity signing the passage from vortex pairs to arrays of vortices can be estimated as $v_d \approx 3.3$ mm/s. Note that, once attached in the chain, localized structures acquire a smaller size along the drift direction. The spatial period of the chain is approximately one half the size of free localized structures, which is also the minimum drift required for the chain formation.

A qualitative explanation of the different observed regimes can be drawn by performing a linear stability analysis, i.s.a., of the model Eqs. (1) and (2). If θ_0 is the homogeneous stationary solution, we take the ansatz $\theta = \theta_0 + \varepsilon\theta_1$, with θ_1 the perturbation satisfying $\partial_t\theta_1 = \sigma\theta_1$ and $\nabla_{\perp}^2\theta_1 = -q^2\theta_1$, $\varepsilon \ll 1$. By substituting the perturbed solution into Eqs. (1) and (2) we obtain the dispersion relation

$$\sigma = -q^2 - 1 - \chi e^{iq_x\Delta x} \cos\left(\Lambda q^2 + \frac{\varphi_0}{2}\right), \quad (3)$$

with $q^2 = q_x^2 + q_y^2$ and the other coefficients as in [28]. In Fig. 5 $\Re(\sigma)$ is plotted against q_x, q_y for various Δx . While for small Δx the most unstable mode, giving the characteristic size of the structures, is only slightly changed when compared to the rest state, for increasing Δx the dispersion relation becomes the more and more anisotropic. At a critical drift a large change occurs, with the most unstable mode along x shifting at almost twice the one along y , corresponding to the chain formation with structures stacked along the drift direction. For certain drifts transverse instabilities occur, with unstable modes along y giving rise to zigzag deformations of the chain. This effect is also observed in the experiment [29]. Note that in the l.s.a. limit the response of the LCLV reduces to that of a Kerr medium; therefore, the above results are expected to be generic for a large class of nonlinear optical systems where translated structures can be obtained.

In conclusion, we have shown that advection of optical localized structures is accompanied by a large deformation of their profile with the emission of optical vortices in their wake. For large translations a qualitative change is observed, with the formation of chains of structures with smaller size along the drift direction. Further studies are

envisaged for a better characterization of this transition, which is reminiscent of the absolute-convective transition in optical instabilities [30]. Similar behaviors could also be observed in the spontaneous motion of localized patterns in delayed feedback resonators [31].

M. G. C. and R. G. R. acknowledge the FONDECYT project 1090045 and 11080286, respectively.

- [1] D. J. Tritton, *Physical Fluid Dynamics* (Oxford University Press, New York, 1988), 2nd ed.
- [2] T. Frisch, Y. Pomeau, and S. Rica, *Phys. Rev. Lett.* **69**, 1644 (1992).
- [3] C. Huepe and M. E. Brachet, *Physica (Amsterdam)* **140D**, 126 (2000).
- [4] K. Sasaki, N. Suzuki, and H. Saito, *Phys. Rev. Lett.* **104**, 150404 (2010).
- [5] See, e.g., N. D. Mermin, *Rev. Mod. Phys.* **51**, 591 (1979).
- [6] Y. Nago *et al.*, *J. Phys. Conf. Ser.* **150**, 032071 (2009).
- [7] S. S. Bulanov *et al.*, *Tech. Phys. Lett.* **34**, 34 (2008).
- [8] P. Couillet, L. Gil, and F. Rocca, *Opt. Commun.* **73**, 403 (1989).
- [9] J. F. Nye and M. V. Berry, *Proc. R. Soc. A* **336**, 165 (1974).
- [10] F. T. Arecchi *et al.*, *Phys. Rev. Lett.* **67**, 3749 (1991).
- [11] F. T. Arecchi *et al.*, *Phys. Rev. Lett.* **70**, 2277 (1993).
- [12] P. L. Ramazza *et al.*, *Europhys. Lett.* **19**, 475 (1992).
- [13] G. A. Swartzlander and C. T. Law, *Phys. Rev. Lett.* **69**, 2503 (1992).
- [14] M. Vaupel, K. Staliunas, and C. O. Weiss, *Phys. Rev. A* **54**, 880 (1996).
- [15] C. Barsi, W. Wan, C. Sun, and J. W. Fleischer, *Opt. Lett.* **32**, 2930 (2007).
- [16] U. Bortolozzo *et al.*, *J. Opt. Soc. Am. B* **26**, 2280 (2009).
- [17] D. R. Solli *et al.*, *Nature (London)* **450**, 1054 (2007).
- [18] A. Montina *et al.*, *Phys. Rev. Lett.* **103**, 173901 (2009).
- [19] M. Tlidi, P. Mandel, and R. Lefever, *Phys. Rev. Lett.* **73**, 640 (1994).
- [20] U. Bortolozzo *et al.*, *Phys. Rev. Lett.* **93**, 253901 (2004).
- [21] P. L. Ramazza, U. Bortolozzo, and L. Pastur, *J. Opt. A* **6**, S266 (2004).
- [22] S. Residori, *Phys. Rep.* **416**, 201 (2005).
- [23] P. L. Ramazza *et al.*, *Phys. Rev. E* **52**, 5524 (1995).
- [24] P. L. Ramazza *et al.*, *Phys. Rev. A* **54**, 3472 (1996).
- [25] P. L. Ramazza, S. Ducci, and F. T. Arecchi, *Phys. Rev. Lett.* **81**, 4128 (1998).
- [26] C. Cleff, B. Gütlich, and C. Denz, *Phys. Rev. Lett.* **100**, 233902 (2008).
- [27] M. G. Clerc, A. Petrossian, and S. Residori, *Phys. Rev. E* **71**, 015205 (2005).
- [28] $\chi = -(\pi/4)(\alpha I_{in} \beta A \sqrt{\Gamma V_{FT}} \sin 2\theta_0) / (\Gamma V_0 + \alpha I_{in} A^2)^{3/2}$, $A = \sqrt{(1/2)(1 - \cos\varphi_0)}$, $\varphi_0 = \beta \cos^2\theta_0$, $\Lambda = -L/(2kl^2)$, $t \rightarrow \tau t$, $x \rightarrow lx$, $y \rightarrow ly$; R. Rojas, Ph.D. thesis, University of Nice-Sophia Antipolis, 2005, <http://tel.archives-ouvertes.fr>.
- [29] F. Haudin, Ph.D. thesis, University of Nice-Sophia Antipolis, 2010.
- [30] E. Louvergneaux *et al.*, *Phys. Rev. Lett.* **92**, 043901 (2004).
- [31] M. Tlidi *et al.*, *Eur. Phys. J. D* **59**, 59 (2010).